Check for updates

Synergistic effect of Si-doping and Fe_2O_3-encapsulation on drug delivery and sensor applications of γ-graphyne nanotube toward favipiravir as an antiviral for COVID-19: A DFT study

Mohammad Amin Asgari [a,*], Nasim Bahmani [b]

[a] *Department of Semiconductors, Materials and Energy Research Center (MERC), P.O. Box 31787-316, Tehran, Iran*
[b] *Materials Science Faculty, Islamic Azad University, Science and Research Branch, Tehran, Iran*

A B S T R A C T

In this work, the behavior of favipiravir (FAV) adsorption on the pristine (2,2) graphyne-based γ-nanotube (GYNT) was theoretically studied. Also, the Si-doped form (Si-GYNT) and its composite with encapsulated Fe_2O_3 (Fe_2O_3@Si-GYNT) were investigated within density functional theory (DFT) calculations, using M05 functionals and B3LYP. It was found that FAV is weakly to moderately adsorb on the bare GYNT and Si-GYNT tube, releasing the energy of 2.2 to 19.8 kcal/mol. After FAV adsorption, the bare tube's electronic properties are changed. Localized impurity is induced at the valence and conduction levels by encapsulating a tiny Fe_2O_3 cluster. As such, the target composite becomes a magnetic material. The binding energy between the Fe_2O_3@Si-GYNT and the FAV molecule becomes substantially stronger (E_{ad} = -25.2 kcal/mol). We developed a drug release system in target parts of body, during protonation in the low pH of injured cells, detaching the FAV from the tube surface. The drug's reaction mechanism with Fe_2O_3@Si-GYNT shifts from covalence in the normal environment to hydrogen bonding in an acidic matrix. The optimized structure's natural bond orbital, quantum molecular descriptors, LUMO, HOMO and energy gap were also investigated. The recovery time can be reduced to less than 10 s by increasing the working temperature properly during the experimental test.

1. Introduction

Favipiravir (FAV) was produced as an anti-influenza medicine and is currently available in Japan. FAV is also being stored for many people as a precaution against new types of influenza. By acting as a chain terminator at the time of viral RNA incorporation, this medicine reduces viral load. In a deadly influenza infection paradigm, the FAV heals all mice, but oseltamivir fails to treat the animals [1,2]. As a result, FAV aids in the treatment of animals suffering from deadly infections. In addition to influenza, FAV has been used with thrombocytopenia to cure illness in humans with the life-threatening severe fever, rabies and Ebola virus and Lassa virus [3,4]. It has a great action in animal studies and benefits anti-RNA virus in vitro. In recent years, the FAV has been widely used against RNA-viral infections of Coronavirus disease (COVID-19) [5, 6]. As a result, creating a method for identifying the drug in biological and environmental samples that is sensitive, accurate, simple, and quick to respond is critical.

Nanomaterials such as multi-wall carbon nanotubes (MWCNTs),

carbon dots, graphene oxide, and graphene have recently attracted a lot of attention for conversion, energy storage, sensor and biological applications [7–19]. Due to the high surface capacity for drug loading, excellent transmit ability via cell membranes, physical stability and great chemical resistance, porous materials have gotten a lot of interest as a drug carrier [20–28]. Refinement or specific helicity synthesis of carbon nanotubes (CNTs) has not been achieved, making the design of electrical devices employing CNTs difficult. As a result, finding or designing novel nanostructured material with a low-dimensional tube-like structure ideal for downsizing electrical devices is both exciting and crucial. The BC_3 [29], BC_2N [30], and graphyne-based nanotubes (GYNT) [31] have all been suggested theoretically, with the γ -GYNTs being the most investigated in terms of electrical and mechanical characteristics [32,33]. Baughman et al. [34] suggested graphyne, a hypothetical carbon allotrope consisting of sp^2- and sp-hybridized carbon atoms. The hexagons connected by acetylenic linkages ($-C≡C-$) are formed by sp^2-hybridized C atoms. The inclusion of acetylenic groups adds a wide range of electrical and optical features
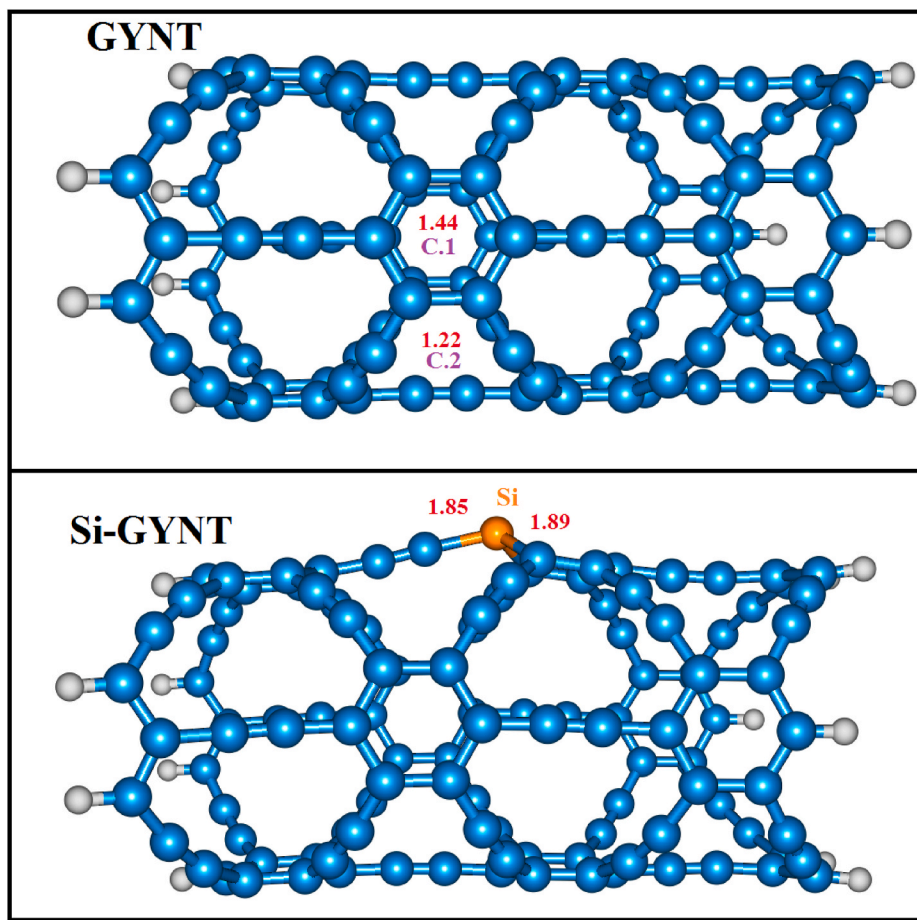
Fig. 1. Optimized structure of GYNT and Si-GYNT. Distances are in Å.
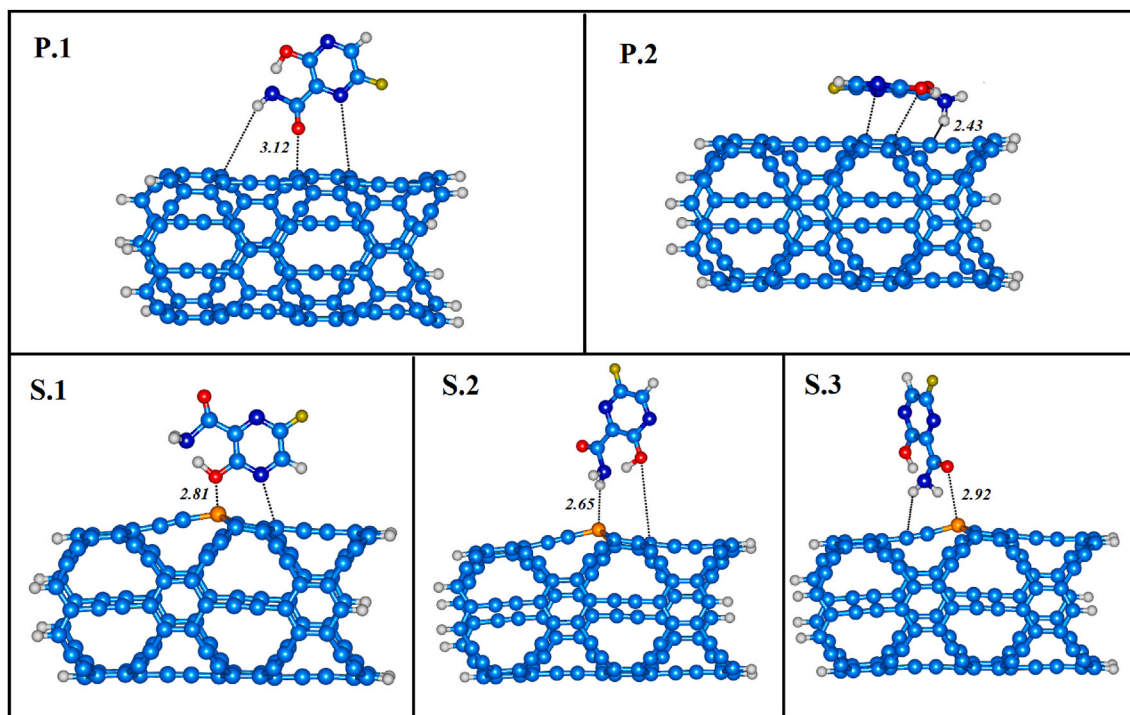

Fig. 2. Models for two stable adsorption states for a FAV molecule on the pristine GYNT three stable adsorption states for a FAV molecule on the Si-GYNT.

Table 1
Adsorption energy (E_{ad} in kcal/mol) and BSSE corrected E_{ad} (E_{BSSE}), HOMO energies (E_{HOMO}), LUMO energies (E_{LUMO}) and HOMO-LUMO energy gap (E_g) of modified systems in eV calculated using B3LYP density functional.

Configuration	E_{ad}	E_{BSSE}	[a]Q_T (|e|)	E_{HOMO}	E_{LUMO}	E_g	[b]ΔE_g (%)	μ	η	ω
GYNT	–	–	–	−4.86	−4.45	0.41	–	−4.65	0.20	52.8
P.1	−16.9	−15.0	0.067	−4.81	−4.44	0.37	9.7	−4.62	0.18	57.8
P.2	−19.8	−17.9	0.109	−4.96	−4.64	0.32	21.9	−4.80	0.16	72.0
Si-GYNT	–	–	–	−4.70	−4.52	0.18	–	−4.61	0.09	118.0
S.1	−2.2	−1.0	0.013	−4.59	−4.40	0.19	5.5	−4.49	0.09	106.3
S.2	−17.0	−15.6	0.167	−4.79	−4.61	0.18	0.0	−4.70	0.09	122.7
S.3	−16.2	−15.8	0.045	−4.78	−4.54	0.24	33.3	−4.66	0.12	90.5
Fe₂O₃@Si-GYNT	–	–	–	−4.85	−4.46	0.39	–	−4.65	0.19	55.5
F.1	−16.1	−14.9	0.138	−4.69	−4.35	0.34	12.8	−4.52	0.17	60.1
F.2	−25.2	−23.8	0.216	−4.86	−4.50	0.36	7.7	−4.68	0.18	60.8

[a] Q_T Q_T is defined as the total NBO charge on the molecule.
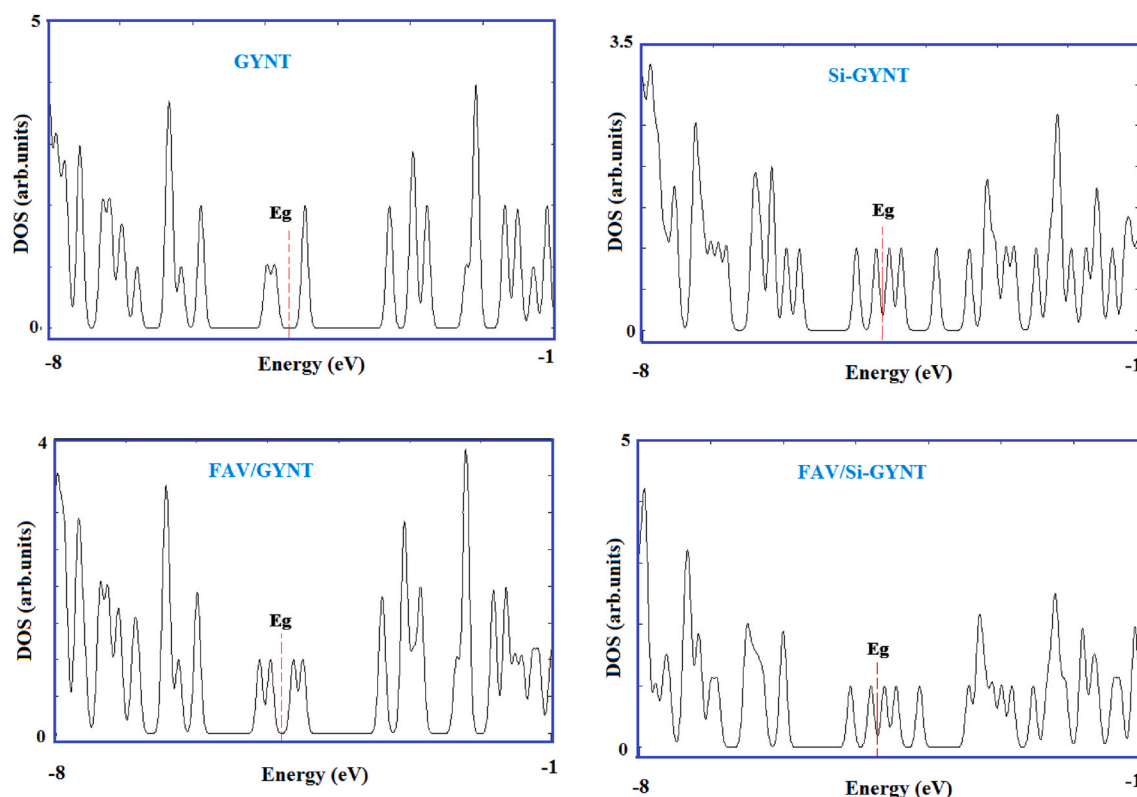[b] Change of E_g of nanotube after FAV adsorption.

Fig. 3. Density of state (DOS) plots of GYNT and Si-GYNT before and after FAV adsorption.

not seen in graphite, such as the natural band gap expansion caused by asymmetric π binds [34].

Recently, different porous materials have been used in biological application such as drug delivery [35–46]. For example, sensing and detection of target analysts with different mechanisms needed synthesis of composites [46–57]. The magnetic materials in this system must only act when the magnetic field is applied, and when the field is eliminated, it becomes inactive. Superparamagnetic nanoparticles having a single domain state smaller than 10 nm are known to have such magnetic characteristics [58,59]. The need to incorporate the benefits of MWCNTs (maximum load ability) and magnetic drug carriers (accurate delivery) to provide more precise medication to give a bigger amount of medication with more precision.

Theoretical investigations were carried out to uncover the mechanisms at work of the successfully fabricated nanostructures delivery system, which can give us some more knowledge about how nanotubes interact with the molecules they transport [60–66]. The interaction of undoped and Si-doped fullerene with FAV was studied by Parlak et al.

[67], and findings reveal the FAV molecule is sensitive to Si-doped fullerene. Rad et al. [68] investigated FAV drug adsorption on the first-row transition metals doped with fullerenes (C_{20}), and revealed Fe, Cr and Ni-doped fullerenes might be used for COVID-19 therapy. The interaction of FAV with γ-GYNTs as a drug carrier will be theoretically studied in this work based on structural, energetic, and electronic characteristics investigations, among other things. The primary purpose of this research is to discover more about how adsorbed molecules affect the features of -GYNTs and how these impacts might be leveraged to develop more effective FAV carrier technologies.

2. Computational methods

From the topology view, in the same way as CNTs, it's feasible to make γ-graphyne nanotubes (γ-GNTs) by turning γ-graphyne sheets into cylinders. Thus, a graphyne sheet consisting of 116 carbon atoms has rolled up, and a (2,2) GYNT resulted, which hydrogen atoms saturated its end atoms to avoid the boundary effects. The calculations on the
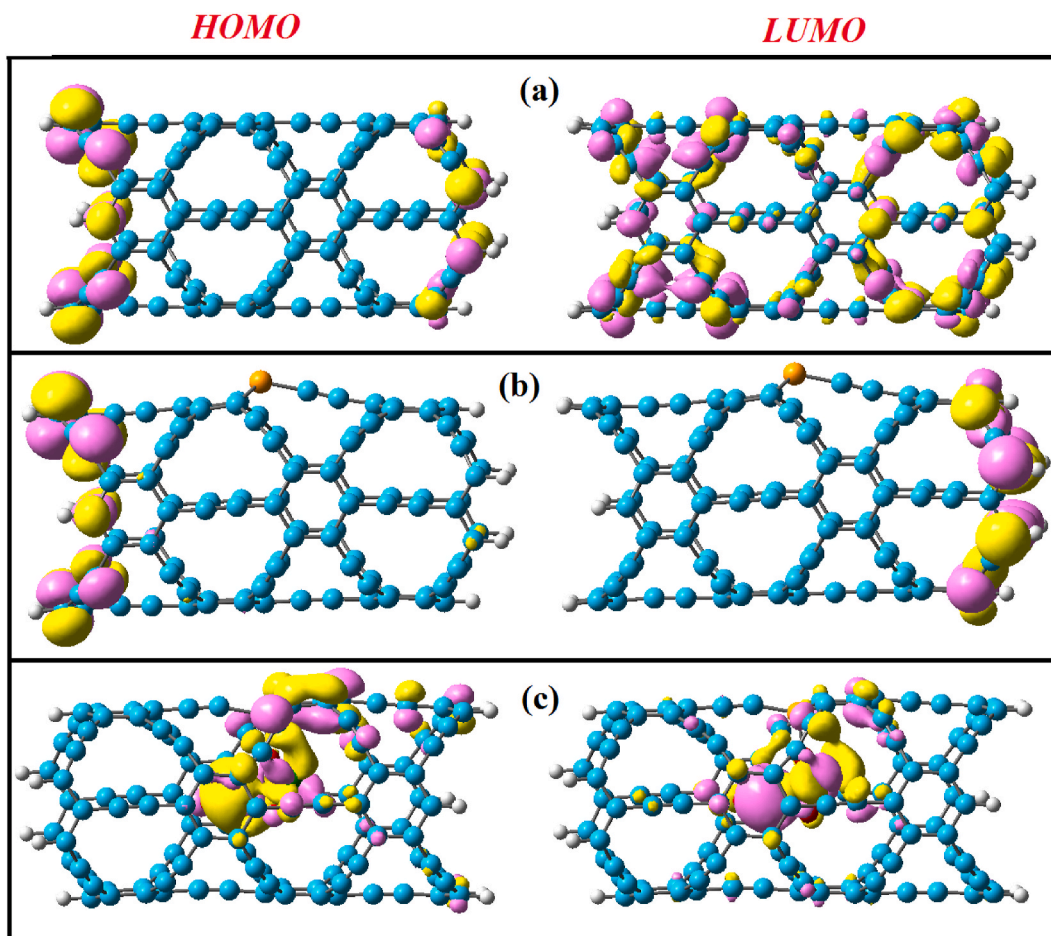
Fig. 4. The HOMO and LUMO patterns of (a) GYNT, (b) Si-GYNT, and (c) Fe$_2$O$_3$@Si-GYNT.
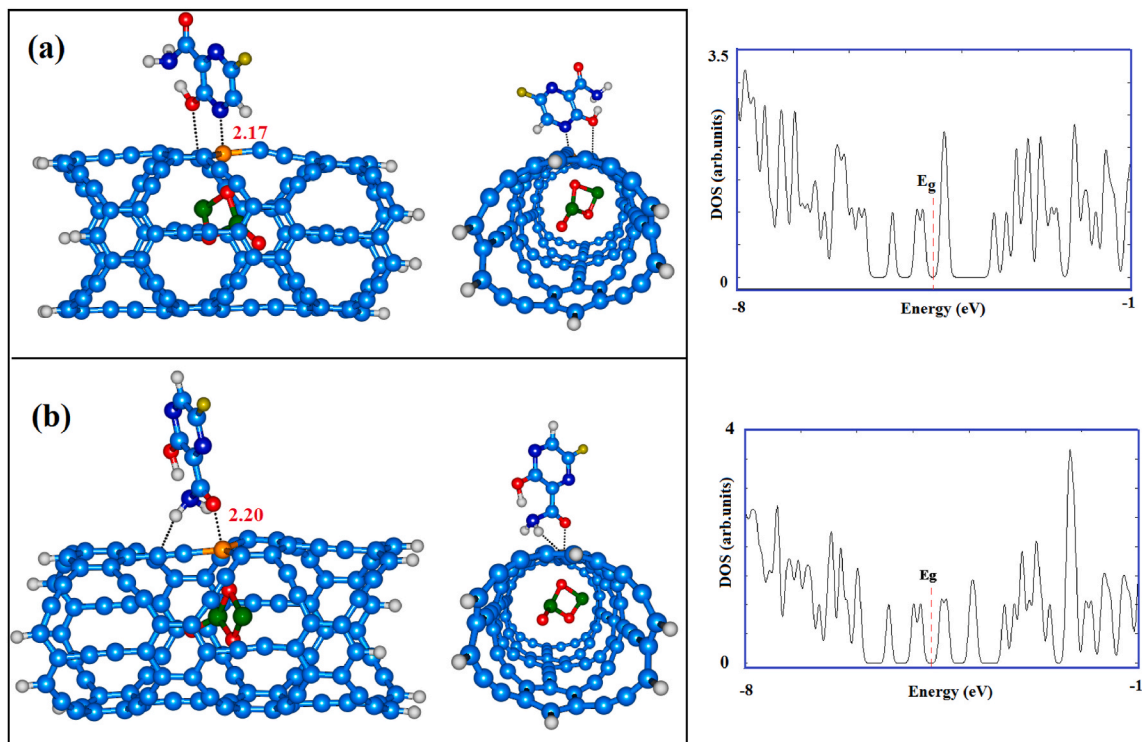

Fig. 5. Top and side views of two stable adsorption states for a FAV molecule on the Fe$_2$O$_3$@Si-GYNT and their density of state (DOS) plots. Distances are in Å.
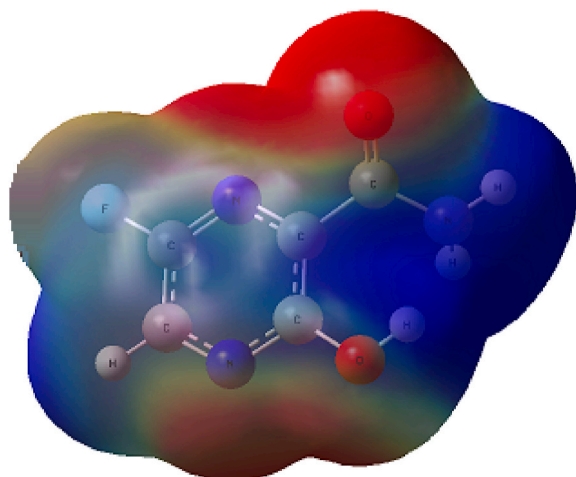
Fig. 6. Computed electrostatic potential on the molecular surface of a single FAV molecule. Color ranges, in a.u.: blue, more positive than 0.010; green, between 0.010 and 0; yellow, between 0 and −0.010; red, more negative than −0.010. (For interpretation of the references to colour in this figure legend, the reader is referred to the Web version of this article.)

pristine, Si-doped GYNT and Fe_2O_3@Si-doped GYNT with and without an AFV molecule were done with the GAMESS software suite's three-parameter hybrid generalized gradient approximation [69] using both the B3LYP function and 6-31G(d)/LANL2DZ mixed basis sets [70]. The density of states (DOS) data were obtained using the GaussSum software [71]. The B3LYP density functional has already been shown to accurately reproduce practical features and is widely utilized in nanostructures [72,73]. The following equation is used to calculate the adsorption energy (E_{ad}) of a FAV molecule on the tube:

$$E_{ad} = E\,(FAV/tube) - E\,(tube) - E\,(FAV) + E_{BSSE} \qquad (1)$$

where E(FAV/tube) , E(tube) and E(FAV) respectively denotes the energy of a nanotube with FAV adsorbed on its surface, denotes the energy of an isolated nanotube and the energy of a single FAV molecule. The negative value of E_{ad} indicates the exothermic nature of the adsorption. Weak interactions were corrected using the basis set superposition error (BSSE). The Fermi level (E_F) is commonly assumed to be roughly in the middle of the energy gap between a molecule's lowest unoccupied molecular orbital (LUMO) and highest occupied molecular orbital (HOMO) (at T = 0 K) (E_g). It's worth noting that the chemical potential is in the center of the E_g. Because the chemical potential of a free gas of electrons is equivalent to its Fermi level as commonly defined, the Fermi level of the systems under study is considered at the center of the E_g.

3. Results and discussion

3.1. Adsorption of FAV on bare and silicon doped GYNT

The atomic structure of GYNT can be represented by substituting –C≡C– linkage for one-third of the carbon-carbon bonds in graphene. There are two non-equivalent carbon atoms in the graphyne network. Fig. 1a illustrates this, sp^2-hybridized (C_1), producing hexagons, and sp-hybridized (C_2), linking the hexagons. The bond length between two sp^2-hybridized carbon atoms is 1.44 in the optimized arrangement and indicating that graphene's -conjugate property is preserved in hexagons. The length of the bond between C_1 and C_2 (1.44 Å) is significantly less than the length of a typical single bond (1.53 Å), showing that they are π-bound together. GYNT is less energetically favorable than CNT due to the presence of two-fold coordinated (sp-hybridized) carbon atoms. The formation of a C≡C triple bond between sp-hybridized carbon atoms in the chain is indicated by the short distance (1.22 Å) between them [74].

The thermal and mechanical stability of -GYNTs has been confirmed through theoretical calculations, and they differ from CNTs in some ways. Because of the higher vibrational mismatch between the strong benzene ring with sp^2 carbon and the weak acetylenic links with sp carbon, Hu et al. [75] found that -GYNTs have an unparalleled low lattice thermal conductivity. According to NBO charge analysis, the predicted excess charge on the atoms of isolated GYNT has an unusual signature. The positive charge ranges from 0.13 to 0.32 e for all sp^2 atoms in the ring, while the negative charge ranges from two acetylenic carbon atoms.

Next, Si-doped GYNT (Si-GYNT) was created by substituting a Si atom for one of the C_1 or C_2 atoms of GYNT's. After a Si atom is doped in C1, the E_{dop} is determined to be +3.79 eV, whereas, for the C_2 doping method, it is found to be +5.46 eV. Because these positive numbers show that both doping techniques are endothermic, C_1 doping may be a more energetically advantageous process than C_2 doping, only C1 doping was explored. When Si impurity replaces C atoms, the geometric structure of the GYNT is significantly changed. The stated atom impurity is thrust out of the tube surface in this configuration to relieve stress due to its larger size than the C atom.

The $Si–C_1$ and $Si–C_2$ bonds in the Si-GYNT have estimated bond lengths of 1.89 and 1.85 Å, respectively, which are significantly longer than the pristine tube's corresponding C–C bonds (Fig. 1b). In addition, the $C_2–C_2–C_1$ angle in the pristine sheet (120°), which is higher than the $C_2–Si–C_1$ angle in the doped sheet is 112°, which the natural bond orbital (NBO) analysis reveals is due to the defect site hybridization changing from sp to almost sp^3. According to the study, around 0.84 e is transferred from the doped silicon to its adjacent carbon atoms within the sidewall, showing that the Si–C bonds in the sidewall are somewhat ionic.

Various initial adsorption geometries are possible, including single (oxygen, flour, nitrogen, or carbon), double (H–N, O–H, or C–O), and

Table 2
Adsorption energy (E_{ad} in kcal/mol), HOMO energies (E_{HOMO}), LUMO energies (E_{LUMO}) and HOMO-LUMO energy gap (E_g) of modified systems in eV calculated using M05 density functional.

Configuration	E_{ad}	[a]Q_T (|e|)	E_{HOMO}	E_{LUMO}	E_g	[b]ΔE_g (%)	μ	η	ω
GYNT	–	–	−4.97	−4.37	0.60	–	−4.67	0.3	36.3
P.1	−24.5	0.051	−4.68	−4.42	0.26	56.6	−4.55	0.13	79.6
PP.2	−22.2	0.095	−4.90	−4.54	0.36	40.0	−4.72	0.18	61.9
Si-GYNT	–	–	−4.75	−4.49	0.26	–	−4.62	0.13	82.1
S.1	−4.1	0.011	−4.69	−4.37	0.32	23.0	−4.53	0.16	64.1
S.2	−20.4	0.178	−4.87	−4.54	0.33	26.9	−4.70	0.16	67.1
S.3	−20.2	0.051	−4.88	−4.46	0.42	61.5	−4.67	0.21	51.9
Fe_2O_3@Si-GYNT	–	–	−4.96	−4.37	0.59	–	−4.66	0.29	36.9
F.1	−19.7	0.148	−4.79	−4.23	0.56	5.1	−4.51	0.28	36.3
F.2	−34.2	0.230	−4.97	−4.43	0.54	8.4	−4.7	0.27	40.9

[a] QT Q_T is defined as the total NBO charge on the molecule.
[b] Change of E_g of nanotube after FAV adsorption.
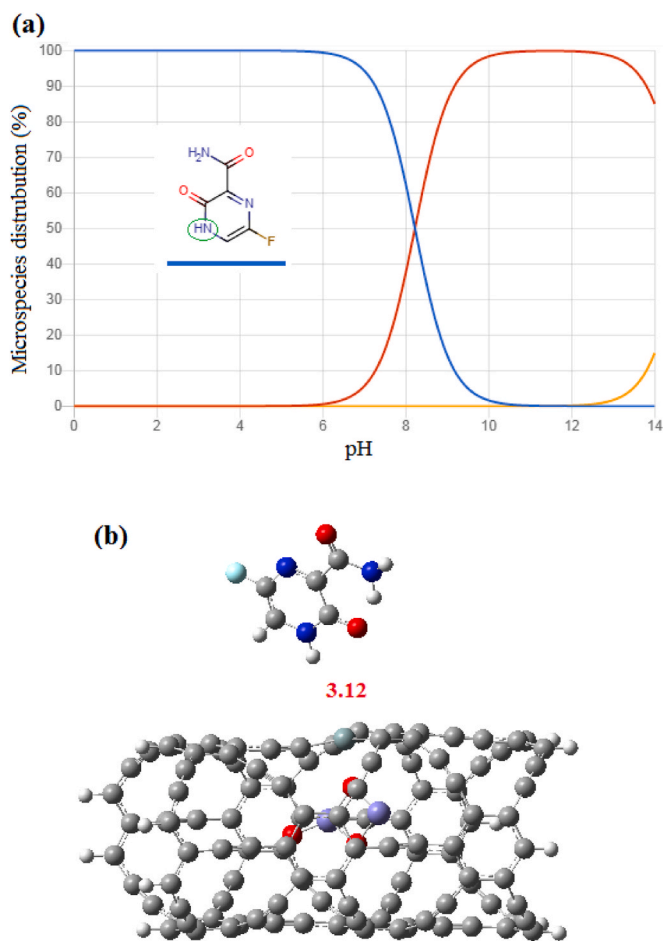
(a)

(b)

Fig. 7. (a) Ionization plot of FAV molecule versus pH. The optimized structure of FAV adsorption on Fe$_2$O$_3$@Si-GYNT in acidic pH.

triple (C–O–H, H–N–H, or N–C–O) bonded atoms to C1 and C$_2$ and Si atoms on different adsorption sites, are considered in obtaining the most stable structure of single FAV adsorbed on the pristine and doped tubes. However, the relaxing method yielded just two and three local minima structures for GYNT and Si-GYNT, respectively (Fig. 2). More data from the calculations of the various FAV/tube structures, which include E$_{ad}$ and E$_g$ configurations, are presented in Table 1. The P.2 configuration (which is the most stable of the FAV/GYNT configurations) represents a van der Waals connection between the FAV molecule and bare GYNT. One of the N–H bonds of the NH$_2$ group is placed on top of the porous site of the tube in this configuration, and the predicted E$_{ad}$ value (Table 1) is around -19.8 kcal/mol, with an equilibrium distance of 2.43 Å. The physical character of the interaction is revealed by the E$_{ad}$ of FAV on the surface in this structure. FAV/Si-GYNT system's most stable configuration (S.2) is one in which the H atoms of NH$_2$ are close to the doped atom, with an equilibrium distance of 2.65 Å and a corresponding E$_{ad}$ of -17.0 kcal/mol, confirming the interaction's weakness. The higher stability of the P.2 configuration in contrast to the S.2 configuration can be explained by the fact that the hexagonal ring in the bare tube is in a good position for π-π interaction with the aromatic ring of FAV. In contrast to bare tube, silicon has damaged the aromaticity of the doped hexagonal ring, making the - interaction between FAV and Si-GYNT unfavorable, from standpoint of drug delivery application. Table 1 indicates that the effect of the BSSE correction on the weaker interaction is larger.

The tube's DOS plots and the FAV/tube complex were calculated to evaluate the effect of adsorption process on the electronic features of different tubes. Calculated DOS and E$_g$ in Table 1 and Fig. 3 indicate that

the pristine GYNT is a semiconductor. The coupling between C (2p$_z$) orbitals yields π conjugate orbitals on the graphyne basal plane, according to the carbon-carbon bond length distribution in graphyne. The dominance of the π -conjugated orbitals over the electrical structure of graphyne is intriguing. The GYNT has a band gap of 0.41 eV, unlike wide-band-gap graphyne sheets. Due to charge transfer, the E$_g$ of the tube reduced from 0.41 eV in the bare tube to 0.37 for P.1 and 0.32 eV for P.2 complexes, as shown in Table 1. The change in electronic feature after FAV adsorption is minor, showing that GYNT/FAV is a semiconductor yet. The DOS plots for silicon doping in Fig. 3c reveal a significant change, suggesting that the electronic characteristics of the GYNT are particularly sensitive to silicon doping, with the E$_g$ of Si-GYNT changing by %57, indicating that Si-GYNT has a metallic nature. As shown in Fig. 3d, after FAV adsorption, both the HOMO and LUMO energies in the instance of S.2 drop to lower energies, but the E$_g$ remains at 0.18 eV. The molecular electrostatic pattern (MEP) of each most stable configurations shown in Fig. S1, confirms different adsorption properties of bare and Si-doped GYNTs.

3.2. Adsorption of FAV on Fe$_2$O$_3$@Si-GYNT

These results imply that the FAV molecule interacts weakly with both clean and doped GYNT, resulting in modest physical adsorption. As a result, the effect of encapsulating magnetic Fe$_2$O$_3$ in Si-GYNT on FAV molecule adsorption is considered. As previously stated, magnetic materials such as Fe$_2$O$_3$ have recently been used extensively to fabricate drug vehicle composites. The encapsulation of a smaller Fe$_2$O$_3$ cluster within the tube cylinder is now considered. The formation energy (E$_f$) is defined by the expression:

$$E_f = E (Fe_2O_3@Si\text{-}GYNT) – E (Si\text{-}GYNT) – E (Fe_2O_3) \qquad (2)$$

where E (Fe$_2$O$_3$@Si-GYNT), E(Si-GYNT), E(Fe$_2$O$_3$) are the total energy of the Si-GYNT with the encapsulated Fe$_2$O$_3$, the silicon doped GYNT, and the free Fe$_2$O$_3$ cluster, respectively. The negative value of E$_f$ = -56.3 kcal/mol suggests that the encapsulation of Fe$_2$O$_3$ is exothermic and thus stable, according to this definition. The HOMO and LUMO patterns of GYNT are still located in whole surface of tube after single silicon doping (Fig. 4), but they shifted to doping site after Fe$_2$O$_3$ encapsulation and it seems the adsorption behavior of tube in composite form is differ from bare and Si-doped form. Following that, we investigated FAV adsorption on the magnetic Fe$_2$O$_3$@Si-GYNT composite by varying the starting orientation of the molecule above the Si atom. As shown in Fig. 5, the studied composite has two distinct adsorptive configurations of FAV. The E$_{ad}$ value of configuration F.1 is -16.1 kcal/mol, which is lower than the E$_{ad}$ value of configuration F.2 (E$_{ad}$ = -25.2 kcal/mol). When contrasted the doped and pure tubes, FAV adsorption on Fe$_2$O$_3$@Si-GYNT is more energetically advantageous. One of the aromatic nitrogen atoms of FAV was placed above the Si atom in configuration F.1, with a bond length of 2.17 Å. Configuration F.2 is more stable than configuration F.1 may be explained by FAV's MEP analysis. Fig. 6 shows the optimized structure of MEP plot for FAV with the formula C$_5$H$_4$N$_3$O$_2$F. It depicts carbonyl oxygen and a –NH$_2$ group as the most likely FAV reaction sites. Interestingly in the case of F.2, both of reaction site are near to tube surface resulted to more favorable adsorption with lengths of 2.20 for O–Si and 2.25 Å for H–C bonds, respectively.

It's worth noting that the DFT approach with the B3LYP functional can't adequately capture the rather weak interactions. However, the primary goal of this study is to compare the adsorption behavior of tubes, not to determine the exact values of E$_{ad}$. However, to explore the effect of dispersion forces and the method utilized on the values of E$_{ad}$, geometrical parameters, and E$_g$, we used the M05 to calculate the aforementioned parameters once more. Among numerous functionals tested, M05 was proposed by Truhlar et al. for general-purpose non-covalent interactions that included both metallic and nonmetallic elements [76]. The obtained results are shown in Table 2, indicating that
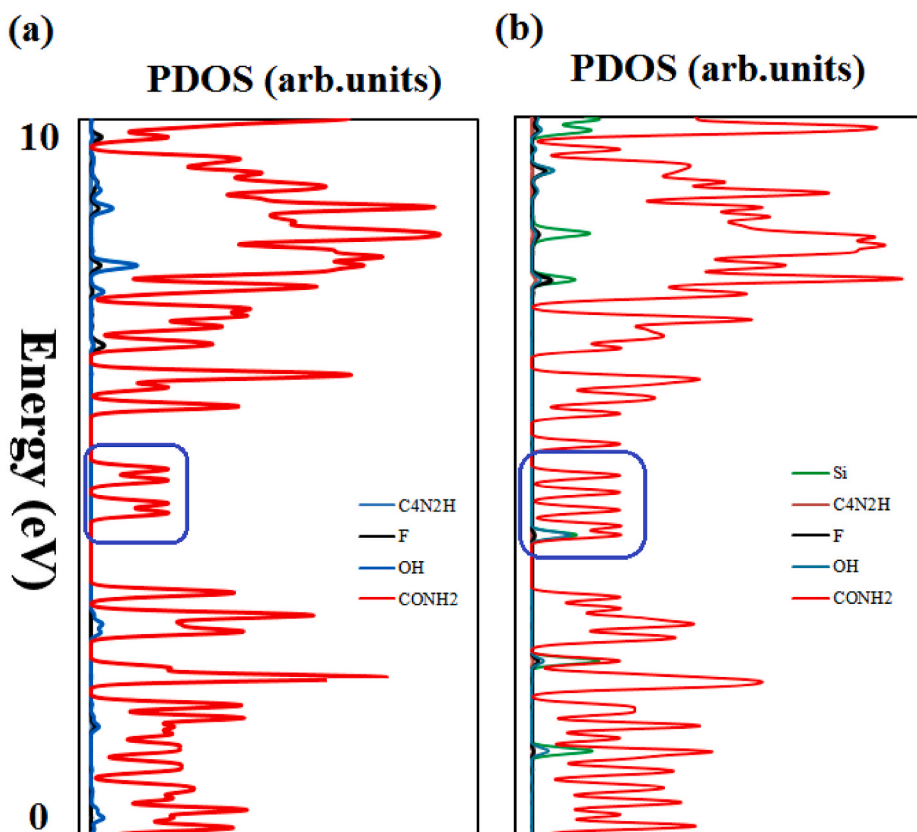
Fig. 8. PDOS plots of (P.2) FAV/GYNT and (S.3) FAV/Si-GYNT.

the Ead acquired using this approach is always higher than the E_{ad} obtained using the B3LYP. The Fe_2O_3@Si-GYNT instance is particularly intriguing since the E_{ad} increases from -25.2 kcal/mol in B3LYP to -34.2 kcal/mol in M05, indicating a 35% increase in energy. It explains that the B3LYP isn't a good way for studying systems that are stabilized due to weak dispersive interactions. For these systems, dispersion-corrected DFT approaches such as the M05 approach produce improved energy properties. As shown in Table 2, these functionals have a strong consistency in estimating the relative magnitude of E_{ad} of the FAV molecule in the examined systems, i.e., the order is Fe_2O_3@Si-GYNT > GYNT > Si-GYNT for both techniques. From standpoint of comparison, the dispersion term has lowest contribution in P.2 structure with 12% improvement, and highest contribution of dispersion term was in S.2 structure by about 86% changing. Also, the electronic properties of structures strongly depend on applied functional, so that as shown in DOS plots of Fig. S2 the E_g changing was improved in M05 system.

3.3. Modified GYNT as a drug delivery vehicle of FAV

To examine the effect of FAV on the reactivity of graphyne-based nanotubes, the electrophilicity index (ω), global hardness (η), and chemical potential (μ) were estimated to explore the reactivities of pristine and FAV adsorbed nanotubes. Tables 1 and 2 demonstrate three DFT-based chemical descriptors for bare and functionalized GYNT, including μ, η, and ω. The mean of HOMO and LUMO energies is determined by η in these numbers is estimated as half of the energy disparities between HOMO and LUMO. The ω used to estimate the molecule's reactivity [77], which is computed using the equation: $\omega = \mu^2/2\eta$. The electrophilic indexes of various chemical substances and the reaction rate in the biochemical process have been discovered to be connected. The electrical index affects the energy stability of a chemical system as it gets extra charges from the environment. Based on the M05 functional, the FAV adsorption on the GYNT resulted in a 0.34 eV

decrease in the HOMO-LOMO gap. The μ and η indexes are reduced by 0.12 and 0.17 eV, respectively, while the ω index is enhanced by 43 eV. The three electrophilic indexes and HOMO-LOMO gap, show no significant changes when the FAV is adsorbed on the optimized Fe_2O_3@Si-GYNT composite. It is subsequently discovered that the chemical stabilities of Fe_2O_3@Si-GYNT are maintained when the drug is adsorbed on the surface, whereas the reactivity of bare GYNT fluctuate considerably.

The Fe_2O_3@Si-GYNT has been shown to be fairly suitable for FAV drug adsorption, which is the first and most important stage in the drug delivery process. However, drug release from the carrier in the target cell is one of the most challenging phases in drug delivery. In fact, tumor cells have a lower pH than normal cells ($\sim$ pH < 6), creating an acidic environment in malignant tissues [78]. We investigated the influence of pH on the most stable compound between the Fe_2O_3@Si-GYNT and the FAV because its pK_a value is 5.1. The H^+ species will tend to link to the nucleophilic heads of the FAV in an acidic matrix (Fig. 7a), causing the H atom of the –OH group to migrate to the neighboring nitrogen atom in the hexagonal ring and protonated (named HFAV). We experimented with different orientations and adsorption locations on the tube surface for HFAV adsorption. After relax structural modifications, re-orientation of the molecule has been anticipated for some cases and one stable HFAV/Fe_2O_3@Si-GYNT complex has been produced (Fig. 7b). The distance between the medication and the tube increases to 3.12 Å in this design with E_{ad} of -7.8 kcal/mol. As shown in Fig. 7b, the interaction is hydrogen bonding-based proton attack which can to split the drug from the carrier. As a result, the drug cannot adhere to the carrier in an acidic environment and has to be released. Thus we think that encapsulation of magnetic Fe_2O_3 besides Si-doping may be a suitable strategy for improving the drug delivery of FAV by GYNT.
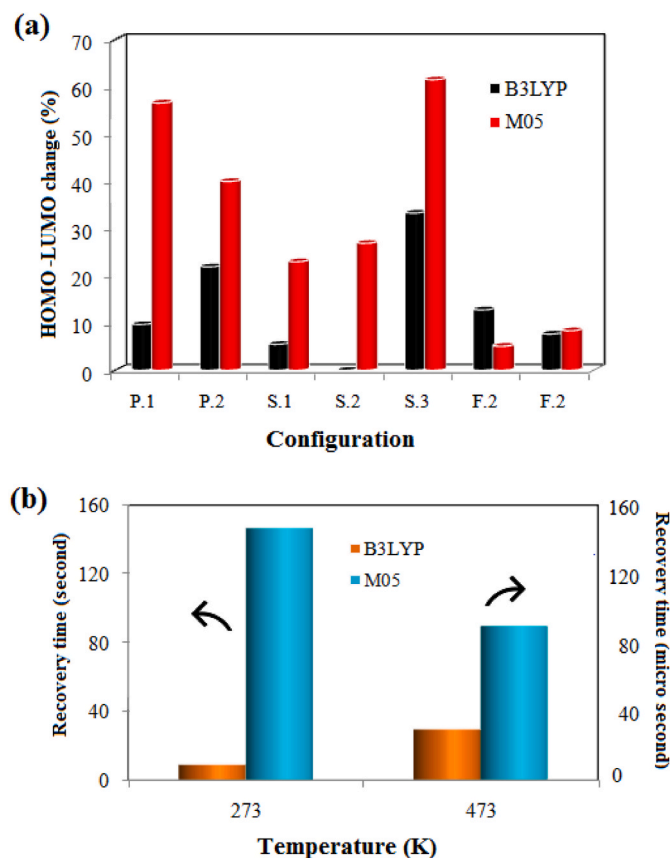
Fig. 9. (a) ΔE_g of each studied tube after FAV adsorption, and (b) recovery time of FAV detection by Si-GYNT (S3 configuration) versus temperature in B3LYP and M05 level of theories.

3.4. Modified GYNT as a FAV sensor

The E_g (or band gap in bulk materials) is a well-known factor in defining a material's electrical conductivity, and there is a typical relationship between them as follows.

$$\sigma \propto \exp(\frac{-E_g}{2kT}) \tag{2a}$$

where σ and k are the electrical conductivity and the Boltzmann's constant, respectively. Smaller E_g at a constant temperature leads to bigger electrical conductivity. Fig. 5 shows the DOS charts for various models of the FAV/Fe$_2$O$_3$@Si-GYNT. It may be deduced that the free Fe$_2$O$_3$@Si-GYNT (Table 1) is a semiconductor material with an E_g of 0.39 eV. Although the FAV molecule has strong contact with the Fe$_2$O$_3$@Si-GYNT, the electrical characteristics of the tube have not altered much, and the E_g of the tube has marginally lowered to 0.36 eV following FAV adsorption. As a result, the associative adsorption of the FAV molecule cannot significantly alter the electrical conductance of the Fe$_2$O$_3$@Si-GYNT. Unlike bare GYNT, The electronic characteristics of the nanotube are particularly sensitive to FAV adsorption, as seen by the DOS plot of Si-GYNT. When comparing the valence level of the doped tube before FAV adsorption to that of the S.3 configuration, it can be seen that the valence level has changed significantly, but the conduction level has remained nearly constant. The E_g was also increased from 0.18 to 0.24 eV (about 33.3% change in B3LYP and 61.5% in M05 level of theory) upon the adsorption of FAV molecule. It appears that Si-GYNT can directly convert the presence of an FAV molecule into an electrical signal, suggesting that it could be employed in FAV sensors. Also, the partial DOS (PDOS) plots of P.2 and S.3 as two most sensitive configurations than FAV drugs are shown in Fig. 8. As can be seen in the PDOS

plots of P.2 structure, the CONH$_2$ group of FAV molecule has the most contribution, but the –OH group has the least intensity. For the S.3 structure, the CONH$_2$ exhibit the highest contribution, the Si atom of nanotube and –F group of drug moderate impartment which influences to better sensing properties of Si-GYNT. The recovery time, which represents the degree of difficulty of adsorbate desorption, is another significant characteristic for drug detection. Short recovery durations are expected for biological molecule detection, which can be determined using weak binding values as given in the equation below.

$$\tau = F_0^{-1} \exp(\frac{-E_{ad}}{K_b T_w}) \tag{3}$$

where τ, is recovery time, F_0 (10^{12} s^{-1}) is attempt frequency, K_b (8.62×10^{-5} eV K^{-1}) is Boltzmann constant and T_w is working temperature [79]. According to this equation, decreasing the adsorption energy decreases the recovery time, which is undesirable. The recovery time versus to temperature and E_g changing of all configurations of are displayed in Fig. 9 with both of B3LYP and M05 functionals. Due to the rapid desorption of FAV molecules at high temperatures, the recovery time lowers as the temperature rises. Although FAV has a short recovery time due to modest adsorption, it can be reduced to less than 10 s by increasing the working temperature properly during the experimental test. As a result, we believe that the Si doping method could be used to improve GYNT's sensitivity to FAV, which the Fe$_2$O$_3$@Si-GYNT cannot detect.

4. Conclusion

DFT calculations are used to study the adsorption of the FAV molecule on pure, Si-doped, and F$_2$O$_3$ encapsulated Si-doped GYNTs. The FAV molecule is observed to be weakly adsorbed on the pure and Si-GYNT tubes, with a lower negative adsorption energy and a significant separation. The highest adsorption energies of FAV in bare and Si-doped GYNT are -19.8 and -.17.0 kcal/mol, respectively. The adsorption of the FAV molecule causes a change in the electronic characteristics of the Si-GYNT about 33% and thus can be a potential sensor for FAV. The FAV molecule, on the other hand, has greater interactions with the Fe$_2$O$_3$@Si-GYNT. The M05 modifies the absolute energy levels of B3LYP results but not their relative order of magnitudes, according to the findings. A short recovery time of <10 s was obtained at higher temperature. Also, in the low pH of cancer tissues, proton attack can detach the FAV from the Fe$_2$O$_3$@Si-GYNT as a potential drug carrier. The hydrogen bonding energy is projected to be relatively low, around -7.8 kcal/mol.

Declaration of competing interest

The authors declare that they have no known competing financial interests or personal relationships that could have appeared to influence the work reported in this paper.

Appendix A. Supplementary data

Supplementary data to this article can be found online at https://doi.org/10.1016/j.jics.2022.100666.

References

[1] Y. Xu, M. Al-Mualm, E.M. Terefe, M.I. Shamsutdinova, M.J.C. Opulencia, F. Alsaikhan, A. Turki Jalil, A.T. Hammid, A. Enayati, H. Mirzaei, V. Khori, A. Jabbari, A. Salehi, A. Soltani, A. Mohamed, Arab. J. Chem. 15 (2022), 103942.
[2] M.U.F. Khan, B.R. Ali, H.Q. Mohammed, H.M.T. Al-Shammari, A. Turki Jalil, N.K. K. Hindi, W. Suksatan, B.Q. Saeed, R.F. Obaid, M.M. Saleh, M.M. Kadhim, Appl. Nanosci. (2022) 1–8.
[3] A.T. Jalil, M. Shanshool, S.H. Dilfy, M. Mahmood Saleh, A.A. Suleiman, J. Microbiol. Biotechnol. Food Sci. 11 (2021) e4229.
[4] H. Qi, Z. Hu, Z. Yang, J. Zhang, J.J. Wu, C. Cheng, C. Wang, L. Zheng, Anal. Chem. 94 (2022) 2812–2819.

[5] M.M. Saleh, A.T. Jalil, R.A. Abdulkereem, A.A. Suleiman, TURKISH J. Immunol. 8 (2020) 129–134.

[6] G. Widjaja, A. Turki Jalil, H. Sulaiman Rahman, W.K. Abdelbasset, D.O. Bokov, W. Suksatan, M. Ghaebi, F. Marofi, J. Gholizadeh Navashenaq, F. Jadidi-Niaragh, M. Ahmadi, Hum. Immunol. 82 (2021) 733–745.

[7] A. Turki Jalil, H. Emad Al Qurabiy, S. Hussain Dilfy, S. Oudah Meza, S. Aravindhan, M.M. Kadhim, A.M. Aljeboree, J. Nanostructures. 11 (2021) 333–346.

[8] M. Rudiansyah, W.K. Abdelbasset, S.A. Jasim, G. Mohammadi, S.M. Dharmarajlu, C. Nasirin, A. Turki Jalil, M.J.C. Opulencia, M. Kadhem Abid, S. Shahbazi Naserabad, Aquaculture 555 (2022), 738254.

[9] A. Fitriyah, D.A. Nikolenko, W.K. Abdelbasset, M.S. Maashi, A.T. Jalil, G. Yasin, M. M. Abdulkadhm, G.U. Samieva, H.A. Lafta, A.M. Abed, L.S. Amaral, Y.F. Mustafa, Chemosphere 301 (2022) 134698.

[10] D. Bokov, A. Turki Jalil, S. Chupradit, W. Suksatan, M. Javed Ansari, I.H. Shewael, G.H. Valiev, E. Kianfar, Adv. Mater. Sci. Eng. 2021 (2021), 5102014.

[11] K. Hachem, S.A. Jasim, M.E. Al-Gazally, Y. Riadi, G. Yasin, A. Turki Jalil, M. M. Abdulkadhm, M.M. Saleh, M.N. Fenjan, Y.F. Mustafa, A. Dehno Khalaji, J. Chin. Chem. Soc. 69 (2022) 512–521.

[12] Z. Tao, L. Huageng, W. Zhen, Q. Chaorui, P.Y. Bo, Z. Xinyu, L. Jiapu, G. Xu, X. Jianbo, H. Xian, T. Junwei, O.-Y. Jun, Y. Xiaofei, L. Fei, Z. Benpeng, Sci. Adv. 8 (2022), eabk0159.

[13] B. Bai, S. Jiang, L. Liu, X. Li, H. Wu, Powder Technol. 387 (2021) 22–30.

[14] S.A. Jasim, J.M. Hadi, M.J.C. Opulencia, Y.S. Karim, A.B. Mahdi, M.M. Kadhim, B. D.O, A.T. Jalil, Y.F. Mustafa, K.T. Falih, J. Alloys Compd. 917 (2022), 165404.

[15] X. Hu, A.H. Derakhshanfard, I. Patra, I. Khalid, A.T. Jalil, M.J.C. Opulencia, R. B. Dehkordi, D. Toghraie, M. Hekmatifar, R. Sabetvand, J. Taiwan Inst. Chem. Eng. 135 (2022) 104396.

[16] X. Cui, C. Li, Y. Zhang, Z. Said, S. Debnath, S. Sharma, H.M. Ali, M. Yang, T. Gao, R. Li, J. Manuf. Process. 80 (2022) 273–286.

[17] H. Li, Y. Zhang, C. Li, Z. Zhou, X. Nie, Y. Chen, H. Cao, B. Liu, N. Zhang, Z. Said, S. Debnath, M. Jamil, H.M. Ali, S. Sharma, Kor. J. Chem. Eng. 39 (2022) 1107–1134.

[18] L. Tang, Y. Zhang, C. Li, Z. Zhou, X. Nie, Y. Chen, H. Cao, B. Liu, N. Zhang, Z. Said, S. Debnath, M. Jamil, H.M. Ali, S. Sharma, Chin. J. Mech. Eng. 35 (2022) 3.

[19] H. Li, Y. Zhang, C. Li, Z. Zhou, X. Nie, Y. Chen, H. Cao, B. Liu, N. Zhang, Z. Said, S. Debnath, M. Jamil, H.M. Ali, S. Sharma, Int. J. Adv. Manuf. Technol. 120 (2022) 1–27.

[20] H. Li, F. Wang, Mater. Des. 204 (2021) 109683.

[21] D. Chen, Y. Li, X. Li, X. Hong, X. Fan, T. Savidge, Chem. Sci. 13 (2022) 8193–8202.

[22] F. Yu, Z. Zhu, C. Li, W. Li, R. Liang, S. Yu, Z. Xu, F. Song, Q. Ren, Z. Zhang, Appl. Catal. B Environ. 314 (2022) 121467.

[23] X. Hu, P. Zhang, D. Wang, J. Jiang, X. Chen, Y. Liu, Z. Zhang, B.Z. Tang, P. Li, Biosens. Bioelectron. 182 (2021) 113188.

[24] S.R. Obireddy, W.-F. Lai, Pharmaceutics 13 (2021) 313.

[25] W.-F. Lai, D. Gui, M. Wong, A. Döring, A.L. Rogach, T. He, W.-T. Wong, J. Drug Deliv. Sci. Technol. 63 (2021), 102428.

[26] Z. Zhuo, Y. Wan, D. Guan, S. Ni, L. Wang, Z. Zhang, J. Liu, C. Liang, Y. Yu, A. Lu, G. Zhang, B.-T. Zhang, Adv. Sci. 7 (2020), 1903451.

[27] S. Ghaffar, M.A. Naqvi, A. Fayyaz, M.K. Abid, K.N. Khayitov, A.T. Jalil, F. Alsaikhan, A.T. Hammid, M.E. Al-Gazally, V. Mohammadparast, B. Jannat, M. Nouri, Compl. Ther. Med. 69 (2022), 102845.

[28] R. Saleh, O. Bokov, M. Fenjan, W. Abdelbasset, U. Altimari, A.T. Jalil, L. Thangavelu, W. Suksatan, Y. Cao, J. Mol. Liq. 352 (2022) 118676.

[29] X. Wang, Comput. Theor. Chem. 1202 (2021), 113299.

[30] J. Jiang, T. Yan, D. Cui, J. Wang, J. Shen, F. Guo, Y. Lin, J. Mol. Liq. 315 (2020), 113741.

[31] Y. Liu, F. Lu, S. Gao, H. Shi, Y. Mai, L. Zhang, Y. Dai, B. Liao, W. Hu, Int. J. Hydrogen Energy 45 (2020), 10797.

[32] J. Ma, Y. Yuan, S. Wu, J.Y. Lee, B. Kang, Appl. Surf. Sci. 531 (2020), 147343.

[33] Y. Yuan, S. Wu, H. Ai, J.Y. Lee, B. Kang, Phys. Chem. Chem. Phys. 22 (2020) 8633.

[34] R.H. Baughman, H. Eckhardt, M. Kertesz, J. Chem. Phys. 87 (1987) 6687.

[35] Y. Yang, M. Yang, C. Li, R. Li, Z. Said, H. Muhammad Ali, S. Sharma, Front. Mech. Eng. (2022), https://doi.org/10.1007/s11465-022-0717-z. In press.

[36] X. Cui, C. Li, Y. Zhang, W. Ding, Q. An, B. Liu, H. Nan Li, Z. Said, S. Sharma, R. Li, S. Debnath, Front. Mech. Eng. (2022), https://doi.org/10.1007/s11465-022-0719-x. In press.

[37] J. Yan, Y. Yao, S. Yan, R. Gao, W. Lu, W. He, Nano Lett. 20 (2020) 5844–5852.

[38] X. Tang, J. Wu, W. Wu, Z. Zhang, W. Zhang, Q. Zhang, W. Zhang, X. Chen, P. Li, Anal. Chem. 92 (2020) 3563–3571.

[39] T. Zhang, Z. Wang, H. Liang, Z. Wu, J. Li, J. Ou-Yang, X. Yang, Y. Peng, B. Zhu, IEEE Trans. Biomed. Eng. (2022) 1.

[40] X. Wang, C. Li, Y. Zhang, H.M. Ali, S. Sharma, R. Li, M. Yang, Z. Said, X. Liu, Tribol. Int. 174 (2022), 107766.

[41] F. Marofi, O. Abdul-Rasheed, H. Rahman, H. setia budi, A.T. Jalil, A. Yumashev, A. Hassanzadeh, M. Yazdanifar, R. Motavalli, M. Chartrand, M. Ahmadi, A. Cid-Arreguid, M. Jarahian, Cancer Sci. 112 (2021).

[42] F. Marofi, H.S. Rahman, Z.M.J. Al-Obaidi, A.T. Jalil, W.K. Abdelbasset, W. Suksatan, A.E. Dorofeev, N. Shomali, M.S. Chartrand, Y. Pathak, A. Hassanzadeh, B. Baradaran, H. Saeedi, S. Tahmasebi, M. Jarahian, Stem Cell Res. Ther. 12 (2021) 465.

[43] S. Moghadasi, M. Elveny, H.S. Rahman, W. Suksatan, A.T. Jalil, W.K. Abdelbasset, A.V. Yumashev, S. Shariatzadeh, R. Motavalli, F. Behzad, F. Marofi, A. Hassanzadeh, Y. Pathak, M. Jarahian, J. Transl. Med. 19 (2021) 302.

[44] A.T. Jalil, W.R. Kadhum, M.U. Faryad Khan, A. Karevskiy, Z.K. Hanan, W. Suksatan, A.S. Waheeb, M.A. Awad, M.M. Abdullah, Iraq, Appl. Nanosci., 2021.

[45] W. Tang, S. Wan, Z. Yang, A.E. Teschendorff, Q. Zou, Bioinformatics 34 (2018) 398–406.

[46] A.T. Jalil, S. Dilfy, A. Karevskiy, N. Mubark, Int.J. Pharm. Res. 12 (2020) 2081–2087.

[47] N. Ngafwan, H. Rasyid, E. Abood, W. Abdelbasset, S. Al-Shawi, D. Bokov, A.T. Jalil, Food Sci. Technol. 42 (2021), e37821.

[48] S. Chupradit, S. Ashfaq, D. Bokov, W. Suksatan, A.T. Jalil, A.M. Alanazi, M. Sillanpaa, Coatings 11 (2021) 1564.

[49] J. Li, Y. Ma, T. Zhang, K. Shung, B. Zhu, BME Front (2022) 1–19, 2022.

[50] T. Li, D. Shang, S. Gao, B. Wang, H. Kong, G. Yang, W. Shu, P. Xu, G. Wei, Biosens 12 (2022) 314.

[51] T. Li, M. Sun, S. Wu, Nanomaterials 12 (2022) 784.

[52] Z. Li, M. Teng, R. Yang, F. Lin, Y. Fu, W. Lin, J. Zheng, X. Zhong, X. Chen, B. Yang, Y. Liao, Sensor. Actuator. B Chem. 361 (2022), 131691.

[53] J. He, P. Xu, R. Zhou, H. Li, H. Zu, J. Zhang, Y. Qin, X. Liu, F. Wang, Adv. Electron. Mater. 8 (2022), 2100997.

[54] T. Li, W. Yin, S. Gao, Y. Sun, P. Xu, S. Wu, H. Kong, G. Yang, G. Wei, The combination of two-dimensional nanomaterials with metal oxide nanoparticles for gas sensors: a review, Nanomaterials 12 (2022) 982.

[55] B. Bai, Q. Nie, H. Wu, J. Hou, Powder Technol. 394 (2021) 1158–1168.

[56] A.T. Jalil, A.H.D. Al-Khafaji, A. Karevskiy, S.H. Dilfy, Z.K. Hanan, Mater. Today Proc. (2021), https://doi.org/10.1016/j.matpr.2021.05.211. In press.

[57] A. Valerievich Yumashev, M. Rudiansyah, S. Chupradit, M.M. Kadhim, A. Turki Jalil, W. Kamal Abdelbasset, W. Suksatan, R. Mireya Romero Parra, Y. Fakri Mustafa, B. Abdullaev, R. Bidares, Anal. Biochem. (2022), 114750, https://doi.org/10.1016/j.ab.2022.114750. In press.

[58] Z. Chen, S. Song, J. Ma, S. Da Ling, Y.D. Wang, T.T. Kong, J.H. Xu, Chem. Eng. Sci. 248 (2022), 117216.

[59] C. Wu, W. Yan, R. Chen, Y. Liu, G. Li, Powder Technol. 397 (2022) 116984.

[60] X. Wu, C. Li, Z. Zhou, X. Nie, Y. Chen, Y. Zhang, H. Cao, B. Liu, N. Zhang, Z. Said, S. Debnath, M. Jamil, H.M. Ali, S. Sharma, Int. J. Adv. Manuf. Technol. 117 (2021) 2565–2600.

[61] S. Chupradit, A.T. Jalil, Y. Enina, D.A. Neganov, M.S. Alhassan, S. Aravindhan, A. Davarpanah, J. Nanomater. 2021 (2021) 3250058.

[62] A. Gowhari Shabgah, Z.M.J. Al-Obaidi, H. Sulaiman Rahman, W. Kamal Abdelbasset, W. Suksatan, D.O. Bokov, L. Thangavelu, A. Turki Jalil, F. Jadidi-Niaragh, H. Mohammadi, K. Mashayekhi, J. Gholizadeh Navashenaq, Clin. Exp. Immunol. 207 (2022) 164–175.

[63] Z.K. Hanan, M.B. Saleh, E.H. Mezal, A. Turki Jalil, Mater. Today Proc. (2021), https://doi.org/10.1016/j.matpr.2021.05.236.

[64] H. Hussein, M. Aubead, H.H. Kzar, Y. Salam, A. Amin, M. Algazally, T. Ahmed, M. Jawad, A. Thaeer Hammid, A.T. Jalil, Y. Mustafa, M. Mahmood Saleh, H. Heydari, Diabetol. Metab. Syndrome 14 (2022) 74.

[65] N. Khaki, S. Fosshat, P. Pourhakkak, R.D. Thanoon, A.T. Jalil, L. Wu, Appl. Biochem. Biotechnol. 194 (2022) 2481–2491.

[66] D. Olegovich Bokov, A.T. Jalil, F.H. Alsultany, M.Z. Mahmoud, W. Suksatan, S. Chupradit, M.T. Qasim, P. Delir Kheirollahi Nezhad, Mol. Simulat. 48 (2022) 438–447.

[67] C. Parlak, Ö. Alver, J. Mol. Struct. 1184 (2019) 110.

[68] A.S. Rad, M. Ardjmand, M.R. Esfahani, B. Khodashenas, Spectrochim. Acta Part A Mol. Biomol. Spectrosc. 247 (2021), 119082.

[69] M.W. Schmidt, K.K. Baldridge, J.A. Boatz, S.T. Elbert, M.S. Gordon, J.H. Jensen, S. Koseki, N. Matsunaga, K.A. Nguyen, S. Su, T.L. Windus, M. Dupuis, J. A. Montgomery, J. Comput. Chem. 14 (1993) 1347.

[70] S. Grimme, J. Comput. Chem. 25 (2004) 1463.

[71] N. O'Boyle, A. Tenderholt, K. Langner, J. Comput. Chem. 29 (2008) 839.

[72] F.A. Saad, N.M. El-Metwally, T.A. Farghaly, M.G. Elghalban, R.K. Shah, G.A. Al-Hazmi, K.A. Saleh, M.Y. Alfaifi, J. Mol. Liq. 229 (2017) 614.

[73] R. Srivastava, F.A.M. Al-Omary, A.A. El-Emam, S.K. Pathak, M. Karabacak, V. Narayan, S. Chand, O. Prasad, L. Sinha, J. Mol. Struct. 1137 (2017) 725.

[74] V.R. Coluci, D.S. Galvão, R.H. Baughman, J. Chem. Phys. 121 (2004) 3228.

[75] M. Hu, Y. Jing X. Zhang, Phys. Rev. B Condens. Matter 91 (2015), 155408.

[76] Y. Zhao, N.E. Schultz, D.G. Truhlar, J. Chem. Theor. Comput. 2 (2006) 364.

[77] H. Xu, L. Li, G. Fan, X. Chu, Comput. Theor. Chem. 1131 (2018) 57.

[78] P. Swietach, R.D. Vaughan-Jones, A.L. Harris, A. Hulikova, Philos. Trans. R. Soc. B 369 (2014), 20130099.

[79] H. Liu, F. Wang, K. Hu, T. Li, Y. Yan, J. Li, Nanomaterials 11 (2021) 100.